lubricants

MDPI

Article

Study of Surface Treatment by Ionic Plasma and Self-Protective Pastes of AISI 304 and 316L Stainless Steels: Chemical, Microstructural, and Nanohardness Evaluation

Francisco Martínez-Baltodano [1], Juan C. Díaz-Guillén [2], Lizsandra López-Ojeda [1], Gregorio Vargas-Gutiérrez [1,*] and Wilian Pech-Rodríguez [3]

[1] Centro de Investigación y de Estudios Avanzados del Instituto Politécnico Nacional, Unidad Saltillo, Ramos Arizpe 25900, Mexico; fco.mtzbaltodano@cinvestav.edu.mx (F.M.-B.); lizsandra.lopez@cinvestav.mx (L.L.-O.)
[2] SECIHTI-InnovaBienestar de México, Saltillo 25290, Mexico; jcarlos@innovabienestar.mx
[3] Department of Advanced Materials, Universidad Politécnica de Victoria, Ciudad Victoria 87138, Mexico; wpechr@upv.edu.mx
* Correspondence: gregorio.vargas@cinvestav.edu.mx; Tel.: +52-8444389600 (ext. 8626)

Abstract: This work studied the effect of self-protective paste nitriding (SPN) and ion plasma nitriding (IPN) on the surface chemistry, microstructure, and nanohardness of AISI 304 and 316L stainless steels, with both treated at 440 °C for 5 h. Surface modifications analyzed using SEM and nanoindentation revealed distinct outcomes. SPN induced an oxynitriding effect due to the oxidation properties of the pastes, forming Fe_3O_4 and Fe_xC phases, while IPN produced an expanded austenite layer. Both methods enhanced surface nanohardness, but SPN showed superior results. For 316L SS, SPN increased nanohardness by 367.81% (6.83 GPa) compared to a 133.5% increase (3.41 GPa) with IPN. For 304 SS, SPN improved nanohardness by 26% (2.23 GPa), whereas IPN reduced it by 48% (0.92 GPa). These findings highlight SPN's potential as an effective anti-wear treatment, particularly for 316L SS. The SPN process utilized a eutectic mixture of sodium cyanate and sodium carbonate, while IPN employed a N_2:H_2 (1:1) gas mixture. SEM analyses confirmed the formation of γ-Fe(N) phases, indicating dispersed iron nitrides (FeN, Fe_3N, Fe_4N). SPN's simultaneous oxidation and nitrocarburization led to an oxide layer above the nitride diffusion layer, enhancing mechanical properties through iron oxides (Fe_3O_4) and carbides (Fe_xC). Comparative analysis showed that AISI 316L exhibited better performance than AISI 304, underscoring SPN's effectiveness for surface modification.

Keywords: surface engineering; mechanical properties; nanohardness; oxynitriding

check for updates

Received: 25 February 2025
Revised: 9 April 2025
Accepted: 22 April 2025
Published: 24 April 2025

Citation: Martínez-Baltodano, F.; Díaz-Guillén, J.C.; López-Ojeda, L.; Vargas-Gutiérrez, G.; Pech-Rodríguez, W. Study of Surface Treatment by Ionic Plasma and Self-Protective Pastes of AISI 304 and 316L Stainless Steels: Chemical, Microstructural, and Nanohardness Evaluation. *Lubricants* **2025**, *13*, 195. https://doi.org/10.3390/lubricants13050195

Copyright: © 2025 by the authors. Licensee MDPI, Basel, Switzerland. This article is an open access article distributed under the terms and conditions of the Creative Commons Attribution (CC BY) license (https://creativecommons.org/licenses/by/4.0/).

1. Introduction

Alloys such as AISI 304 and AISI 316L stainless steels are versatile and commonly used due to their availability, cost-effectiveness, and excellent general corrosion resistance across several environments [1,2]. However, stainless steels remain vulnerable to wear and localized corrosion, particularly under harsh conditions like seawater exposure where localized corrosion (e.g., pitting and crevice corrosion) can compromise their natural passive film [3]. Several methods have been explored to improve the wear and corrosion resistance of stainless steel, but enhancing wear resistance often compromises corrosion protection [4]. Given the superior wearability of chromium nitrides and expanded austenite, this study investigates the effects of two surface treatment processes on the chemical composition, microstructure, and nanohardness of AISI 316L and 304 SS surfaces.

Among the most promising nitriding techniques are self-protecting nitriding pastes (SNPs) [5] and ionic plasma nitriding (IPN) [6,7]. These processes are designed to modify the surface layer's composition and structure, significantly boosting the resistance of stainless steels to both corrosion and wear, while maintaining their inherent mechanical strength.

SNP involves the controlled introduction of oxygen and nitrogen into the surface of the material through solid-phase diffusion, using a self-protecting paste composed of a eutectic mixture of sodium cyanate and sodium carbonate. According to López-Ojeda et al. [5], these self-protecting pastes act as a barrier, preventing direct contact between the metal substrate and the furnace atmosphere during thermochemical treatment. This process results in a marked increase in corrosion resistance and surface hardness.

IPN employs ionic plasma to diffuse nitrogen into the material's surface, offering a suitable alternative method for the surface modification of iron alloys. IPN has been extensively studied in the literature. For instance, Shabashov et al. [8] explored the nitriding of metastable austenitic stainless steels Kh19N8T and Kh17N8GT at various temperatures using IPN with an electron beam used as plasma generation. Their work demonstrated that nitriding at 500 °C induced phase transformations and nitride formation in Kh19N8T steel, while nitriding at 350 °C resulted in a nitride-rich surface layer. These findings underscore the potential of electron beam nitriding to enhance surface hardness, wear resistance, and corrosion resistance in austenitic SS. IPN treatment is known to enhance mechanical properties by introducing nitrogen into the austenite, which significantly increases the lattice parameter and generates substantial residual stresses in the matrix. These stresses facilitate nitrogen diffusion during nitriding, thereby hardening austenitic SS and improving their corrosion resistance [9–11]. For high erosion–corrosion resistance of SS, research efforts look for expanded austenite (γ-Fe(N)) on the surface without the precipitation of chromium nitrides at the grain boundaries. One alternative to achieving this aim is via low-temperature (<450 °C) plasma nitriding [12,13]. Previous studies [13–16] indicated that the formation of the γ-Fe(N) phase occurs after prolonged nitriding at approximately 450 °C. Additionally, other authors suggest that the γ-Fe(N) phase typically emerges between 350 and 400 °C during nitriding of austenitic SS [17,18]. This phase formation is characterized by nitrogen content in the interstitial solid solution ranging from 5 to 30 atomic percent, resulting in approximately 13% expansion of the austenite crystal lattice, which results in enhanced hardness and increased resistance to wear [19–21].

However, their initial investment, the degree of control required, their maintenance and operation expenses, and the limitations for nitriding big-size parts are challenges for the widespread dissemination of this technology.

Because of the excellent resistance to wear of chromium nitrides, Fe_3O_4, and the expanded austenite, the main objective of this research work was to study the effect of two surface treatment processes that allow increasing wear resistance without impairing the resistance to pitting corrosion, with both processes carried out at 440 °C for 5 h. These parameters were selected based on previous studies that reported effective formation of γ-Fe(N) [13–16]. The processes analyzed are the IPN [22,23] and the SPN [5]. Using techniques such as SEM, XRD, and nanohardness testing, the chemical, microstructural, and wear resistance differences were analyzed for these two processes.

This study differs from the previous literature by making a systematic comparison between two nitriding techniques, ionic plasma nitriding (IPN) and self-protecting nitriding paste (SNP), under identical conditions (440 °C, 5 h). This analysis allows a direct evaluation of their impact on the microstructure, as well as the nanohardness and resistance to localized corrosion of AISI 304 and 316L steels. Unlike previous work that looks at these methods separately, our research explicitly addressed the critical balance between wear resistance

(associated with expanded austenite, γ-Fe(N), and chromium nitrides) and the preservation of pitting resistance, a key aspect for applications in aggressive environments. In addition, while the literature has focused on temperatures below 400 °C or above 450 °C to avoid nitride precipitation, this work explored an intermediate range (440 °C) to optimize γ-Fe(N) formation without compromising corrosion protection. In addition, this study assessed the scalable potential of SNP—a less studied but economically viable alternative to IPN—providing comparative data on its effectiveness in surface modification and its industrial applicability for large parts. The results are supported by a comprehensive analysis using SEM, XRD, and nanohardness tests, integrating chemical, microstructural, and mechanical aspects that are usually treated in a fragmented way in the literature.

2. Materials and Methods

2.1. Materials

Substrates of AISI 304 and 316L SS, with diameters of 38.1 mm, were employed for the study. Before experimentation, these substrates were metallographically prepared and polished using sandpaper ranging from 80 to 1000 grit until a mirror-like finish was achieved. The chemical composition of these substrates, as depicted in Table 1, was determined via atomic emission spectrometry.

Table 1. Chemical composition of AISI 304 and AISI 316L SS.

Element / Sample	Elemental Chemical Composition (wt%)									
	C	**S**	**P**	**Si**	**Mn**	**Mo**	**Ni**	**Cr**	**Fe**	**Others**
AISI 304 SS	0.04	0.005	0.052	0.5	1.36	0.138	7.7	18.12	68.2	3.88
AISI 316L SS	0.015	0.014	0.044	0.24	1.68	1.76	9.56	18.04	68.0	0.64

2.2. Surface Treatment with Self-Protecting Paste (SNP)

The SNP treatment was carried out using a self-protecting paste formulated with 65 wt% NaCNO, 25 wt% Na_2CO_3, and 10 wt% carboxymethylcellulose (CMC). In molar terms, the composition corresponds to approximately 78.7% NaCNO, 18.6% Na_2CO_3, and 2.7% CMC. The samples were heated from room temperature to the nitriding temperature of 440 °C at a controlled rate of 3 °C/min in an electric furnace to ensure homogeneous heating, followed by a 5 h isothermal treatment. Immediately after extraction from the furnace, the samples underwent a controlled quenching process in preheated water maintained at 66 °C to stabilize the surface phases (particularly expanded austenite) formed during nitriding. Subsequent surface preparation involved mechanical polishing with 3 μm diamond paste, thorough ultrasonic cleaning in deionized water, and final drying using convective air flow.

2.3. The Ionic Plasma Nitriding (IPN) Process

The IPN process was conducted within a laboratory reactor where the system was evacuated to achieve a pressure of 1.3 Pa. Before processing, the samples were subjected to a cleaning step in an ultrasonic acetone bath. The samples were heated from room temperature to the nitriding temperature of 440 °C at a controlled rate of 3 °C/min. Nitriding was performed at 440 °C for 5 h, applying a sustained discharge current of 270 mA in a gas mixture consisting of 50% N_2 and 50% H_2, which was maintained at 266 Pa pressure. To ensure precise temperature control, a conductive heating system equipped with a K-type thermocouple was used, with the thermocouple in direct contact with the sample. Following heating, the samples were gradually cooled to room temperature within the vacuum chamber in an inert argon atmosphere.

2.4. Surface Characterization

CuKα radiation (λ = 1.5418 Å) was utilized for XRD analysis, operating at a voltage of 40 kV and a current of 30 mA. The diffraction scans were performed with a step size of 0.02° (2θ) per second in a Rigaku Model IV diffractometer. The samples were mounted in epoxy resin (Struers EpoFix, Ballerup, Denmark) and allowed to polymerize for 24 h at 25 °C to ensure adhesion and prevent mechanical damage. They were then roughened with SiC paper (up to 1200 grit) and polished with 1 μm and 0.3 μm alumina slurries until scratch-free surfaces were achieved. Following that, they were ultrasonically cleaned in ethanol for 20 min to remove polishing residue. Finally, they were coated with a 5 nm layer of Au-Pd using a Quorum Q150T ion coater (Quorum, San Jose, CA, USA), thereby improving electrical conductivity and image quality in the FE-SEM (TESCAN MIRA 3). Additionally, nanohardness (H) and Young's modulus (E) measurements of the surface were conducted using a nanoindenter from the RTec instrument (San Jose, CA, USA).

3. Results

3.1. X-Ray Diffraction Analysis

Figure 1 illustrates the diffractograms of untreated, SNP, and IPN AISI 316L SS samples. The untreated sample shows the (111), (200), and (220) peaks related to the single-phase austenite structure in the positions 2θ = 43.57°, 50.75°, and 74.60° (ICDD No. 52-0513). The analysis confirms that γ-Fe (FCC) austenite is the only crystalline phase detected in these samples. In the SNP and IPN samples, the formation of expanded austenite γ-Fe(N) is also evidenced by a shift of the diffraction peaks towards lower angles, consistent with a lattice expansion induced by nitrogen incorporation. This nitrogen-stabilized phase retains the same FCC structure and space group $Fm\bar{3}m$ (No. 225), but it exhibits a larger lattice parameter in the range of a ≈ 3.65–3.80 Å due to interstitial nitrogen occupying octahedral sites and causing local distortion of the crystal lattice.

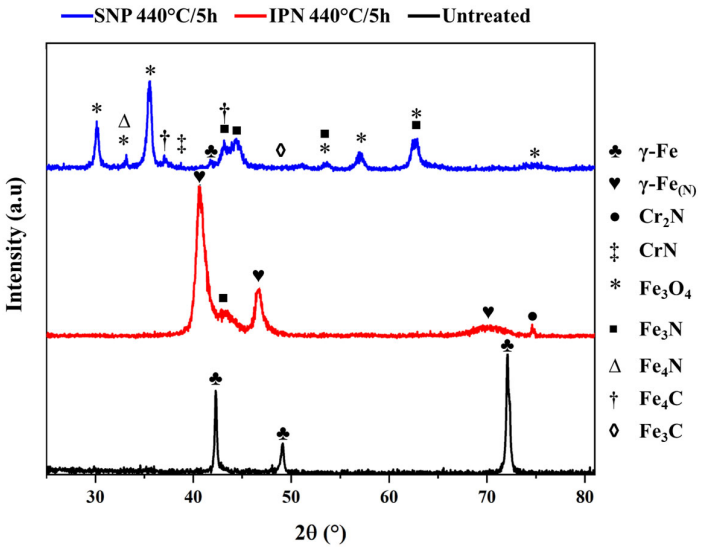


Figure 1. Diffractograms for untreated 316L SS, as well as for after oxynitriding by SNP and nitriding by INP at 440 °C for 5 h.

The primary phases observed in the SNP samples correspond to magnetite (Fe_3O_4), identified by their characteristic diffraction peaks at the following 2θ positions: 30.15° for the (220) plane, 35.51° for (311), 37.15° for (222), 53.55° for (422), 57.09° for (511), 62.69° for (440), 65.92° for (531), and 74.17° for (533) (JCPDS No. 75-0033; 39-1346) [24,25]. Fe_3O_4 crystallizes in a cubic inverse spinel structure with space group $Fd\bar{3}m$ (No. 227) and a

lattice parameter of a = 8.39 Å, where Fe^{3+} ions are distributed among both octahedral and tetrahedral sites, contributing to its magnetic and electrical properties. Additionally, the diffraction peaks for Fe_3N were found at 44.21°, 69.98°, and 78.21°, corresponding to the (111), (103), and (212) planes, respectively. Fe_3N exhibits a hexagonal crystal structure with space group $P6_322$ (No. 182) and lattice parameters a = 4.72 Å and c = 4.38 Å, with interaxial angles $\alpha = \beta = 90°$ and $\gamma = 120°$, which are characteristic of its hexagonal symmetry. The diffraction peak for Fe_4N was found at 49.63°, corresponding to the (200) plane (JCPDS No. 01-1236) [26].

Peaks corresponding to Fe_3C were found at positions of 49.11° for the (221) plane, and Fe_4C at positions of 37.16° and 49.52° for the (110) and (112) planes, respectively (JCPDS No. 01-1236; ICSD 18-7143). Fe_4C, also known as cementite, crystallizes in an orthorhombic structure with space group Pnma (No. 62) and lattice parameters a = 5.09 Å, b = 6.74 Å, and c = 4.52 Å, with interaxial angles $\alpha = \beta = \gamma = 90°$. This phase is commonly formed during surface treatments involving carbon diffusion and contributes to increased hardness and brittleness of the modified layer. The presence of this compound is relevant since it confirms the formation of a compound that is only reached at high temperatures, as shown with Liu et al. (2016) [27] who carburized 308 SS at temperatures between 800 and 1100 °C. However, many reports in the literature have shown that low-temperature carburization is possible as reported by Ernst et al., whose work consisted of exposing an AISI 316L SS sheet to 474 °C to achieve carburization [28]. Other authors, such as Maistro et al. [29], reported carburization of 304 SS at temperatures below 500 °C. They explained that carburization is possible thanks to the longer exposure time, which allows more carbon atoms to diffuse into the surface of the steel. Carbides within the modified surface layer influence the tribomechanical properties and corrosion resistance of the treated components [30]. In the IPN samples, the presence of the γ-Fe(N) phase was mainly detected. Additionally, small peaks of Cr_2N and Fe_3N were observed.

Figure 2 presents the diffractograms for untreated, SNP, and IPN AISI 304 SS samples. For untreated samples, the only phase detected is γ-Fe (austenite), which exhibits a face-centered cubic (FCC) structure with space group $Fm\bar{3}m$ (No. 225) and a lattice parameter in the range of a = 3.59–3.65 Å, depending on the alloy composition. This phase is stabilized at room temperature by the presence of Ni and other austenite-stabilizing elements.

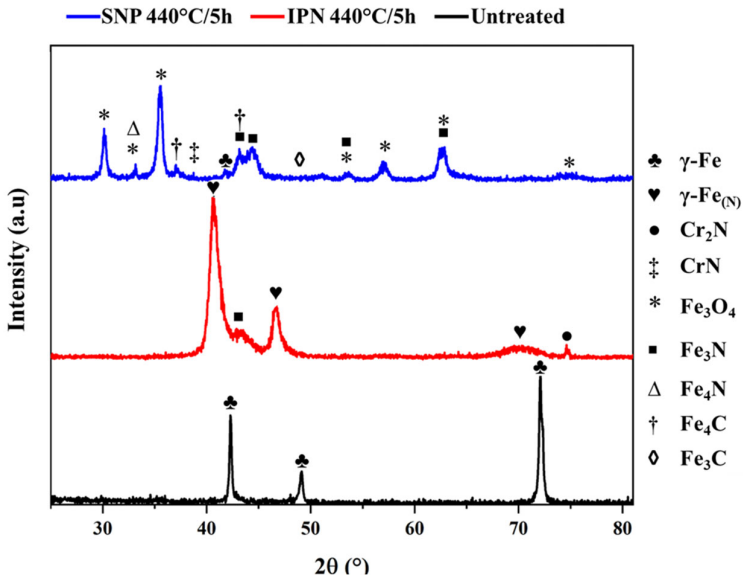


Figure 2. Diffractograms for untreated 304 SS, as well as for after oxynitriding by SNP and nitriding by INP at 440 °C for 5 h.

In the SNP samples, the phases identified were iron nitrides (Fe_4N, Fe_3N), magnetite (Fe_3O_4), and chromium nitrides (Cr_2N). Fe_4N exhibited a distorted perovskite-like cubic structure with space group $Pm\bar{3}m$ (No. 221) and a lattice parameter of a = 3.79 Å, while Fe_3N had a hexagonal structure with space group $P6_322$ (No. 182) and lattice parameters a = 4.72 Å, c = 4.38 Å, typical of nitrogen-rich phases. Fe_3O_4 (magnetite) crystallized in a cubic inverse spinel structure with space group $Fd\bar{3}m$ (No. 227) and a lattice parameter of a = 8.39 Å, where Fe^{3+} occupied both octahedral and tetrahedral sites. Additionally, weak diffraction peaks corresponding to Cr_2N were observed at 37.6° and 75.6°, attributed to the (111) and (311) planes, respectively. Cr_2N crystallized in a hexagonal close-packed (HCP) structure with space group $P\bar{3}1m$ (No. 164), lattice parameters a = 4.76 Å, c = 4.42 Å, and nitrogen atoms occupying interstitial sites.

For the IPN samples, both γ-Fe and expanded austenite γ-Fe(N) phases were detected. The presence of the original γ-Fe (FCC) phase likely originated from the subsurface region (second modified layer), while the top layer exhibited γ-Fe(N), formed by nitrogen diffusion. γ-Fe(N) retained the FCC structure and space group $Fm\bar{3}m$ (No. 225) but displayed a lattice expansion of a ≈ 3.65–3.80 Å due to interstitial nitrogen incorporation into octahedral sites. This was evidenced by a shift in the (111) diffraction peak to 41.05°, the (200) to 46.35°, and a significant broadening in the (220) region between 67° and 71°. The broadening suggests the presence of crystalline defects such as dislocations, vacancies, or interstitial impurities, which disrupt the periodicity of the crystal lattice and reduce long-range order.

3.2. Microstructure Analysis

Figures 3 and 4 show the micrographs of the cross-section of the SNP samples. SNP treatment developed a two-layer structure that, according to EDS analysis, consists of a top oxide layer (Fe_3O_4, Cr_2O_3), followed by a nitrogen- and carbon-rich layer.

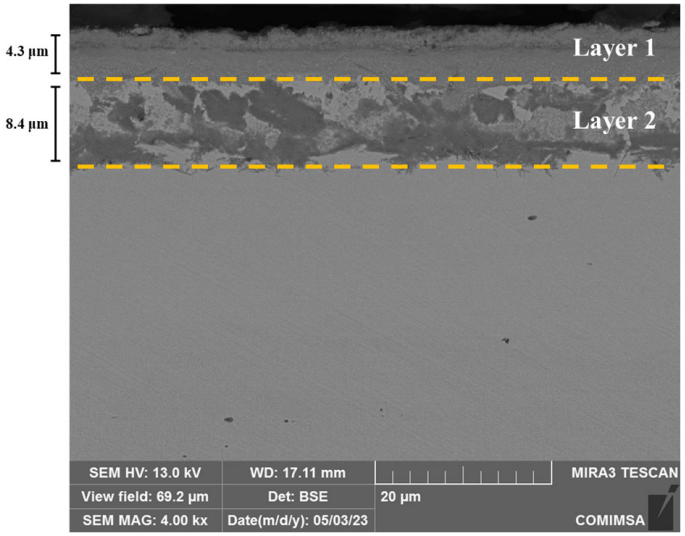


Figure 3. Micrograph of the cross-section and EDS analysis of AISI 316L SS oxynitrided by SNP at 440 °C for 5 h.

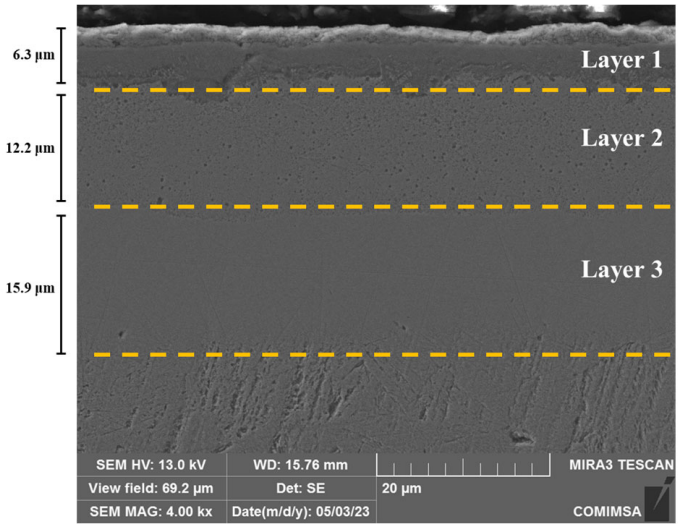


Figure 4. Micrograph of the cross-section and EDS analysis of AISI 304 SS oxynitrided by SNP at 440 °C for 5 h.

Atomic nitrogen was formed from the dissociation reaction of CNO^-, as shown by Equation (1) [31].

$$4CNO^- \rightarrow 2CN^- + {CO_3}^{2-} + \boldsymbol{CO} + [\boldsymbol{N}] \quad (1)$$

Carburization is also promoted by the release of atomic carbon species according to the CO dissociation reaction shown by Equation (2).

$$\boldsymbol{CO} \rightarrow CO_2 + [\boldsymbol{C}] \quad (2)$$

According to the EDS analyses shown in Table 2, the presence of oxygen in SNP treatment is higher in the first layer due to the formation of Cr and Fe oxides. However, the nitrogen content is lower near the surface, which may be due to the consumption of nitrogen atoms in layer two.

Table 2. Elemental composition of cross-section layers of AISI 316L and AISI 304 SS modified by SNP process at 440 °C for 5 h (Figure 3).

Chemical Composition by EDS, wt%	316L by SNP		304 by SNP	
	Layer 1	Layer 2	Layer 1	Layer 2
Fe	23.19	7.31	22.01	48.2
Cr	15.48	26.31	13.47	14.37
O	50.29	9.61	48.98	1.62
Ni	6.24	1.06	3.34	5.08
N	3.58	24.15	2.56	13.37
C		28.11	8.79	16.51
Mo	0.83	2.95		
Other	0.39	0.5	0.84	0.86

In the case of SNP treatment of AISI 316L, it can be observed in Table 2 that layer 2 is enriched with Mo; this is very important because this chemical element mitigates passivity breakdown and favors repassivation or self-repair [32,33]. This is due to several factors related to the interaction of this element with the chemical and thermal processes that occur during treatment, one of which is selective diffusion, since molybdenum, being an element of higher atomic weight and with low mobility at typical treatment temperatures, tends to diffuse more slowly than other elements such as chromium or iron. Jauberteau

et al. [34] and Zhang et al. [35] claimed that molybdenum has a strong tendency to form stable compounds, such as molybdenum carbides (MoC) and molybdenum nitrides (MoN), during oxynitriding treatment. These compounds can precipitate on or near the surface, contributing to the enrichment of Mo in these areas.

Figures 5 and 6 present the SEM images and Table 3 the elemental analysis of the cross-section of the IPN treatment for both AISI 316L and 304 SS. The IPN samples show a double-layer structure: (i) the composite layer, which is made up of iron–chromium, nickel, molybdenum, oxygen, and nitrogen, and (ii) the nitrogen diffusion layer constituted by a solid solution of nitrogen in austenite. In the 304 SS steel sample, a small increase in the thickness of the diffusion layer is observed compared to the 316L SS steel, due to a higher diffusion rate and depth of nitrogen [36].

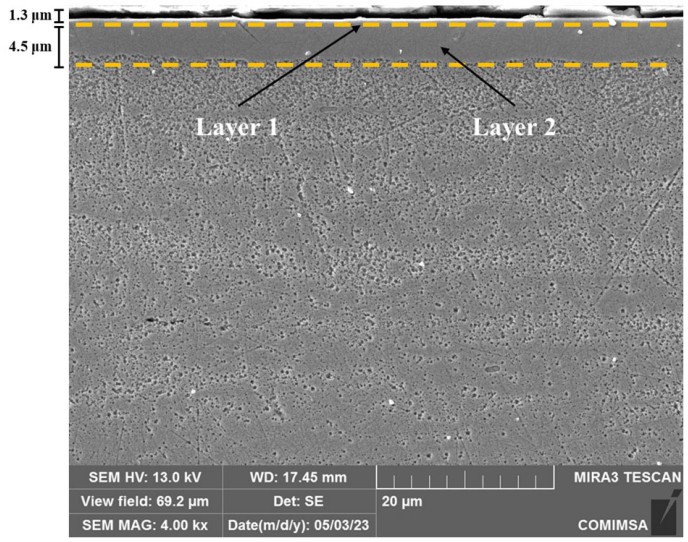


Figure 5. Micrograph of the cross-section and EDS analysis of AISI 316L SS nitrided by IPN at 440 °C for 5 h.

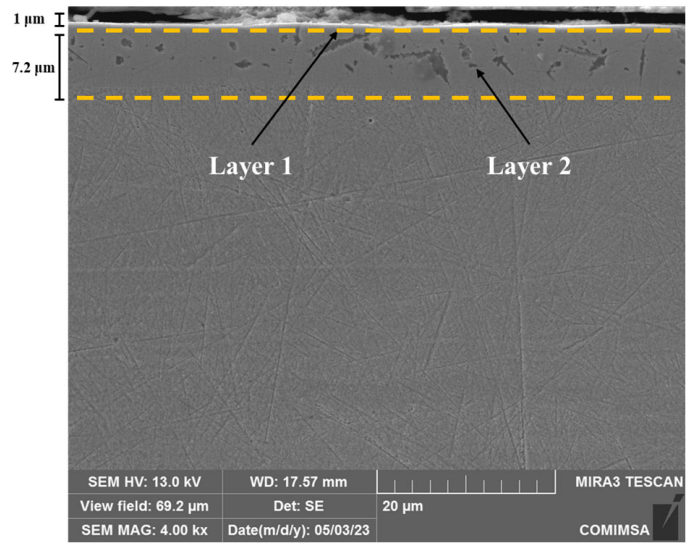


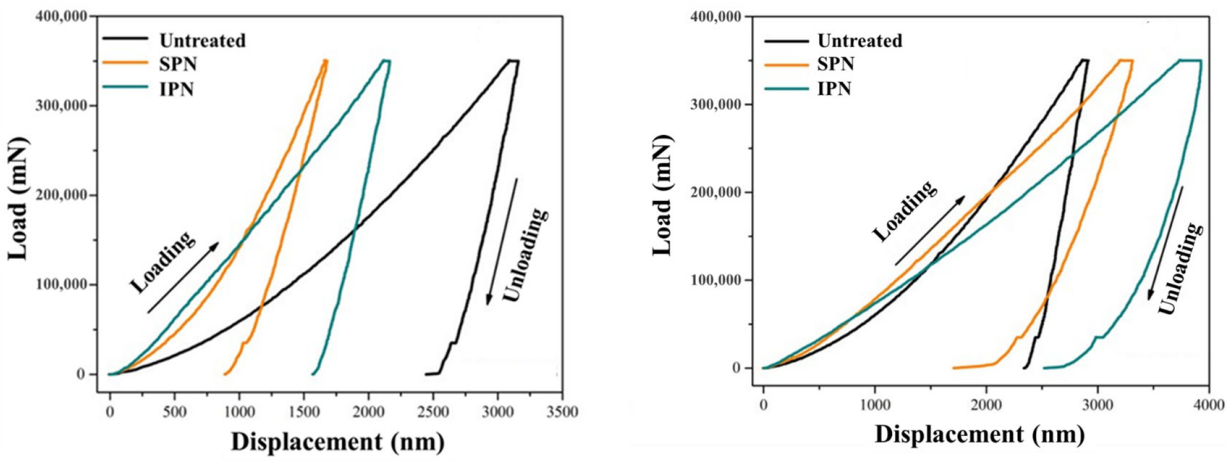
Figure 6. Micrograph of the cross-section and EDS analysis of 304 SS nitrided by IPN at 440 °C for 5 h.

Table 3. Elemental composition of cross-section layers of AISI 316L and AISI 304 SS modified by IPN process at 440 °C for 5 h (Figure 4).

Chemical Composition by EDS, wt%	316L by IPN		304 by IPN	
	Layer 1	Layer 2	Layer 1	Layer 2
Fe		60.93		61.88
Cr		15.39		17.71
O				
Ni		8.07		6.35
N		13.96		12.98
C				
Mo		1.05		
Other		0.6		1.08

3.3. Mechanical Properties

The mechanical properties of the surface layer of unmodified and treated steel samples were assessed through nanoindentation tests. Figure 7 displays the load–displacement curves, with loading and unloading phases marked by arrows. A plastic factor (η_p), representing the ratio of the work of plastic deformation (W_p) to the total deformation work (W_t), was calculated [36]. The measured values of nanohardness (H), elastic modulus (E), η_p, W_p, W_t, and the H/E ratio are detailed in Table 4. Notably, the H/E ratio is a dimensionless parameter that serves as an indirect measure of a material's strength and is particularly relevant to the wear resistance of hard materials. Physically, it reflects the material's resistance to plastic deformation and its capacity to sustain elastic strain before failure—commonly referred to as "elastic strain to failure [37].



(**a**) (**b**)

Figure 7. Load–displacement curves of steel samples for untreated (black line), SNP (orange line), and IPN (green line) samples: (**a**) 316L SS; (**b**) 304 SS.

Table 4. Mechanical properties of AISI 316L and 304 SS: nanohardness, elastic modulus, and deformation work in untreated, SPN-, and IPN-treated samples.

Sample	Nanohardness, H (GPa)	Elastic Modulus, E (GPa)	Plastic Factor, η_p (%)	Plastic Deformation, W_p (nJ)	Total Deformation, W_t (nJ)	H/E
Untreated 316L SS	1.46	92.6	87.44	336.53	384.84	0.015
316L SS by SPN	6.83	140.98	58.61	96.85	165.23	0.048
316L SS by IPN	3.41	130.76	82.52	240.62	291.58	0.026
Untreated 304 SS	1.77	115.01	87.67	288.4	328.94	0.015
304 SS by SPN	2.23	43.11	64.68	235.97	364.82	0.051
304 SS by IPN	0.92	38.75	83.47	480.82	576	0.024

For 316L SS, both SNP and IPN treatments resulted in increased nanohardness and modulus values compared to the untreated steel. Specifically, the nanohardness of 316L SS increased by 367.81% from SNP treatment and by 133.56% IPN treatment. The oxynitrided surface exhibited higher nanohardness values relative to plasma nitride surfaces, owing to the formation of oxynitrides, metal carbides, chromium oxide, and magnetite. Conversely, for 304 SS, no significant increase in nanohardness by IPN was observed on the surface compared to the untreated surface. However, a hardening effect of 26% was evident on the surface by SNP treatment, due to the formation of nitrides, oxynitrides, carbides, and complex oxides that reinforce the surface layer. Given that a higher H/E ratio typically correlates with increased wear resistance [38], it suggests that SNP-treated surfaces exhibit superior mechanical strength. The increased nanohardness of SNP samples might come from the balance achieved between carbide formation, oxynitride deposition, and the formation of a complex oxide layer on the surface of AISI 316L SS.

The measured hardness of the treated material exhibited a marked increase relative to values reported in prior studies. For example, Jeyakymar et al. [39] proposed a nitrocarburizing process for 316L SS where the best mean harness was 241.25 HV (2.366 GPa), delivered by the sample being carburized at 590 °C for 135 min. Attabi et al. [40] used the ball burnishing treatment for 316L SS and the higher reported microhardness was 542.2 HV (5.317 GPa), which was smaller than the value of 6.83 GPa obtained by the SNP process in this work. This effect has also been reported in the literature, specifically the transformation from the γ-austenite phase to the α'-martensite phase, as well as the reverse transformation of α'-martensite. These phase transitions lead to variations in both hardness and elastic modulus [41].

4. Conclusions

The self-protective paste nitriding (SPN) process resulted in the formation of an oxidized surface layer composed of Fe_3O_4, Fe_xC, Fe_xN, and Cr_2N, significantly enhancing surface nanohardness compared to ion plasma nitriding (IPN). For AISI 316L stainless steels, SPN increased nanohardness by 367.81%, achieving 6.83 GPa, while IPN yielded a 133.56% increase, reaching 3.41 GPa. In contrast, for AISI 304 stainless steel, SPN improved nanohardness by 25.99% (2.23 GPa), whereas IPN reduced it by 48.02% (0.92 GPa). IPN formed an expanded austenite layer on both plates of steel, with γ-Fe(N) phases contributing to nanohardness improvements. However, SPN's superior performance, particularly on 316L SS, underscores its effectiveness in surface hardening, attributed to the synergistic effects of oxidation and nitrocarburization. These results highlight SPN as a promising anti-wear treatment for stainless steel.

Author Contributions: Conceptualization, G.V.-G.; investigation, F.M.-B., J.C.D.-G. and L.L.-O.; data curation, F.M.-B.; methodology, G.V.-G. and J.C.D.-G.; writing—original draft, L.L.-O. and F.M.-B.; writing—review and editing, G.V.-G., J.C.D.-G. and W.P.-R.; funding acquisition, G.V.-G. All authors have read and agreed to the published version of the manuscript.

Funding: This research was funded by the "Secretaría de Ciencia, Humanidades, Tecnología e Innovación" (Secihti) for their support through the Frontier Science Project 2019-845101.

Data Availability Statement: The original contributions presented in the study are included in the article material. Further inquiries can be directed to the corresponding author.

Acknowledgments: We wish to express our gratitude to the "Secretaría de Ciencia, Humanidades, Tecnología e Innovación" (Secihti) for their support through the Frontier Science Project 2019-845101, "Accelerated Discovery of Antibiofouling Materials". F.M.-B. and L.L.O also thank Secihti for the Ph.D. scholarship granted to them.

Conflicts of Interest: Author Juan C. Díaz-Guillén was employed by the company SECIHTI-InnovaBienestar de México. The remaining authors declare that the research was conducted in the absence of any commercial or financial relationships that could be construed as a potential conflict of interest.

Abbreviations

The following abbreviations are used in this manuscript:

SS	Stainless steel
SNP	Self-Protective Paste Nitriding
IPN	Ion Plasma Nitriding
H/E	Hardness-to-Elastic Modulus Ratio

References

1. Dhaiveegan, P.; Elangovan, N.; Nishimura, T.; Rajendran, N. Corrosion behavior of 316L and 304 stainless steels exposed to industrial-marine-urban environment: Field study. *RSC Adv.* **2016**, *6*, 47314–47324. [CrossRef]
2. Rajesh, K.D.; Buddi, T.; Kanth, P.R.; Satyanarayana, K. Microstructural and corrosion resistance study on plasma arc welded joints of AISI 304 and AISI 316. *Adv. Mater. Process. Technol.* **2020**, *6*, 189–205. [CrossRef]
3. Zheng, Z.; Zheng, Y.G. Effects of surface treatments on the corrosion and erosion-corrosion of 304 stainless steel in 3.5% NaCl solution. *Corros. Sci.* **2016**, *112*, 657–668. [CrossRef]
4. Kim, I.-J. Wear Behaviours and Mechanisms. In *Engineering Metrology for Pedestrian Falls Prevention and Protection*; Springer International Publishing: Berlin/Heidelberg, Germany, 2022; pp. 153–191. [CrossRef]
5. López-Ojeda, L.; Vargas-Gutiérrez, G. High wear resistance and better pitting corrosion resistance of AISI 316L stainless steel by a self-protective oxy-nitrocarburizing paste. *J. Mater. Res. Technol.* **2022**, *16*, 1803–1813. [CrossRef]
6. Sah, J.; Joseph, A.; Jhala, G.; Mukherjee, S. On the Effects of H2 and Ar on Dual Layer Formed by Plasma Nitrocarburizing on Austenitic Stainless Steels. *J. Mater. Eng. Perform.* **2022**, *31*, 2664–2677. [CrossRef]
7. Zhang, Z.; Wang, Z.; Shao, M.; Dou, H.; He, Y.; Li, Y.; Luo, J. Structural and tribological properties of sulfonitrocarburizing layers prepared by plasma nitrocarburizing and low temperature ion sulfurizing. *Surf. Coat. Technol.* **2024**, *478*, 130470. [CrossRef]
8. Shabashov, V.A.; Gavrilov, N.V.; Kozlov, K.A.; Makarov, A.V.; Titova, S.G.; Voronin, V.I. Structure of the Surface Layers of Metastable Austenitic Stainless Steel Nitrided in Electron Beam Plasma. *Phys. Met. Metallogr.* **2018**, *119*, 755–763. [CrossRef]
9. Galdikas, A.; Moskalioviene, T. The anisotropic stress-induced diffusion and trapping of nitrogen in austenitic stainless steel during nitriding. *Metals* **2020**, *10*, 1319. [CrossRef]
10. Shen, L.; Wang, L.; Xu, J.J. Plasma nitriding of AISI 304 austenitic stainless steel assisted with hollow cathode effect. *Surf. Coat. Technol.* **2013**, *228*, S456–S459. [CrossRef]
11. Jafarpour, S.M.; Dalke, A.; Biermann, H. Different approaches for plasma nitrocarburizing of austenitic stainless steel using a plasma-activated solid carbon precursor in a hot-wall reactor. *Mater. Res. Technol.* **2025**, *34*, 1791–1802. [CrossRef]
12. Kurelo, B.C.E.S.; Lepienski, C.M.; de Oliveira, W.R.; de Souza, G.B.; Serbena, F.C.; Cardoso, R.P.; das Neves, J.C.K.; Borges, P.C. Identification of Expanded Austenite in Nitrogen-Implanted Ferritic Steel through In Situ Synchrotron X-ray Diffraction Analyses. *Metals* **2023**, *13*, 1744. [CrossRef]

13. Jimenez, L.B.V.; Umemura, M.T.; Calderón-Hernández, J.W.; Magnabosco, R.; Pinedo, C.E.; Tschiptschin, A.P. Plasma nitriding of 410S ferritic/martensitic stainless steel: Microstructure, wear and corrosion properties. *Tecnol. Metal. Mater. Min.* **2023**, *20*, e2830. [CrossRef]
14. Pye, D. *Practical Nitriding and Ferritic Nitrocarburizing*; ASM International: Materials Park, OH, USA, 2003.
15. Yuan, X.; Zhao, Y.; Li, X.; Chen, L. Effects of Gas Nitriding Temperature on the Surface Properties of a High Manganese TWIP Steel. *Metals* **2017**, *7*, 102. [CrossRef]
16. Kurelo, B.C.E.S.; Monteiro, J.F.H.L.; de Souza, G.B.; Serbena, F.C.; Lepienski, C.M.; Cardoso, R.P.; Brunatto, S.F. Thermal Evolution of Expanded Phases Formed by PIII Nitriding in Super Duplex Steel Investigated by In Situ Synchrotron Radiation. *Metals* **2024**, *14*, 1396. [CrossRef]
17. Wang, J.; Wang, J.; Lin, Y.; Yan, J.; Zeng, D.-Z.; Huang, R.; Hu, Z. Modification of AISI 304 Stainless Steel Surface by the Low Temperature Complex Salt Bath Nitriding at 430 °C. *ISIJ Int.* **2012**, *52*, 1118–1123. [CrossRef]
18. Gontijo, L.C.; Machado, R.; Casteletti, L.C.; Kuri, S.E.; Nascente, P.A.P. X-ray diffraction characterisation of expanded austenite and ferrite in plasma nitrided stainless steels. *Surf. Eng.* **2010**, *26*, 265–270. [CrossRef]
19. Christiansen, T.; Somers, M.A.J. Decomposition kinetics of expanded austenite with high nitrogen contents. *Int. J. Mater. Res.* **2006**, *97*, 79–88. [CrossRef]
20. Manova, D.; Lotnyk, A.; Mändl, S.; Neumann, H.; Rauschenbach, B. CrN precipitation and elemental segregation during the decay of expanded austenite. *Mater. Res. Express* **2016**, *3*, 066502. [CrossRef]
21. Monteiro, W.A.; Pereira, S.A.L.; Vatavuk, J. Nitriding Process Characterization of Cold Worked AISI 304 and 316 Austenitic Stainless Steels. *J. Metall.* **2017**, *2017*, 1052706. [CrossRef]
22. Nishimoto, A.; Amano, R.; Tamiya, T. Duplex treatment of active screen plasma nitriding and amorphous hydrogenated carbon coating. *Appl. Surf. Sci. Adv.* **2021**, *6*, 100129. [CrossRef]
23. Li, G.Y.; Lei, M. Microstructure and properties of plasma source nitrided AISI 316 austenitic stainless steel. *J. Mater. Eng. Perform.* **2016**, *26*, 418–423. [CrossRef]
24. Bhosale, M.A.; Ummineni, D.; Sasaki, T.; Nishio-Hamane, D.; Bhanage, B.M. Magnetically separable γ-Fe_2O_3 nanoparticles: An efficient catalyst for acylation of alcohols, phenols, and amines using sonication energy under solvent free condition. *J. Mol. Catal. A Chem.* **2015**, *404–405*, 8–17. [CrossRef]
25. Singh, H.; Kour, S.; Selvaraj, M. Magnetically separable template assisted iron nanoparticle for the enhancement of latent fingerprints. *J. Indian Chem. Soc.* **2022**, *99*, 100661. [CrossRef]
26. Naeem, M.; Díaz-Guillén, J.C.; Khalid, A.; Guzmán-Flores, I.; Muñoz-Arroyo, R.; Iqbal, J.; Sousa, R.R.M. Improved wear resistance of AISI-1045 steel by hybrid treatment of plasma nitriding and post-oxidation. *Tribol. Int.* **2022**, *175*, 107869. [CrossRef]
27. Liu, C.; Chen, X.; Chen, T.; Nie, D.; Wang, L. Carbide transformation in carburised zone of 25Cr35NiNb+MA alloy after high-temperature service. *Mater. High Temp.* **2016**, *33*, 98–104. [CrossRef]
28. Ernst, F.; Cao, Y.; Michal, G.M.; Heuer, A.H. Carbide precipitation in austenitic stainless steel carburized at low temperature. *Acta Mater.* **2007**, *55*, 1895–1906. [CrossRef]
29. Maistro, G.; Yao, Y.; Klement, U.; Nyborg, L.; Cao, Y. On surface carbides in low-temperature carburized austenitic stainless steels. *Mater. Charact.* **2020**, *167*, 110462. [CrossRef]
30. McMurdie, H.F.; Morris, M.C.; Evans, E.H.; Paretzkin, B.; Wong-Ng, W.; Hubbard, C.R. Standard X-Ray Diffraction Powder Patterns from The JCPDS Research Associateship. *Powder Diffr.* **1986**, *1*, 265–275. [CrossRef]
31. Li, L.; Wang, J.; Yan, J.; Duan, L.; Li, X.; Dong, H. The Effect of Liquid Nitriding on the Corrosion Resistance of AISI 304 Austenitic Stainless Steel in H2S Environments. *Metall. Mater. Trans. A* **2018**, *49*, 6521–6532. [CrossRef]
32. Maurice, V.; Marcus, P. Molybdenum effects on the stability of passive films unraveled at the nanometer and atomic scales. *NPJ Mater. Degrad.* **2024**, *8*, 3. [CrossRef]
33. Wang, Z.; Paschalidou, E.-M.; Seyeux, A.; Zanna, S.; Maurice, V.; Marcus, P. Mechanisms of Cr and Mo Enrichments in the Passive Oxide Film on 316L Austenitic Stainless Steel. *Front. Mater.* **2019**, *6*, 232. [CrossRef]
34. Jauberteau, I.; Bessaudou, A.; Mayet, R.; Cornette, J.; Jauberteau, J.L.; Carles, P.; Merle-Méjean, T.J.C. Molybdenum nitride films: Crystal structures, synthesis, mechanical, electrical and some other properties. *Coatings* **2015**, *5*, 656–687. [CrossRef]
35. Zhang, Z.; Li, X.; Dong, H. Response of a molybdenum alloy to plasma nitriding. *Int. J. Refract. Met. Hard Mater.* **2018**, *72*, 388–395. [CrossRef]
36. Li, Y.; He, Y.; Xiu, J.; Wang, W.; Zhu, Y.; Hu, B. Wear and corrosion properties of AISI 420 martensitic stainless steel treated by active screen plasma nitriding. *Surf. Coat. Technol.* **2017**, *329*, 184–192. [CrossRef]
37. Yang, Y.; Guo, J.H.; Yan, M.F.; Zhu, Y.D.; Zhang, Y.X.; Wang, Y.X. Improvement of wear resistance for carburised steel by Ti depositing and plasma nitriding. *Surf. Eng.* **2018**, *34*, 132–138. [CrossRef]
38. Yang, Y.; Zhou, X.; Dai, X.Z.; Li, J.; Zhang, S.H.; Zhang, C.S.; Ding, J.C.; Zheng, J. Comparative study of plasma nitriding and plasma oxynitriding for optimal wear and corrosion resistance: Influences of gas composition. *J. Mater. Res. Technol.* **2021**, *15*, 448–459. [CrossRef]

39. Jeyakymar, M.; Munusami, V.; Shanmugam, P.; Boopalan, N.; Boopathi, S.; Sureshkumar, M. An investigation on wear loss and hardness of nitro-carburizing coated stainless-steel grade-316. *Mater. Today Proc.* **2022**, *66*, 1398–1404. [CrossRef]
40. Attabi, S.; Himour, A.; Laouar, L.; Motallebzadeh, A. Mechanical and wear behaviors of 316L stainless steel after ball burnishing treatment. *J. Mater. Res. Technol.* **2021**, *15*, 3255–3267. [CrossRef]
41. Cios, G.; Tokarski, T.; Żywczak, A.; Dziurka, R.; Stępień, M.; Gondek, L.; Marciszko, M.; Pawłowski, B.; Wieczerzak, K.; Bała, P. The Investigation of Strain-Induced Martensite Reverse Transformation in AISI 304 Austenitic Stainless Steel. *Met. Mater. Trans. A* **2017**, *48*, 4999–5008. [CrossRef]

Disclaimer/Publisher's Note: The statements, opinions and data contained in all publications are solely those of the individual author(s) and contributor(s) and not of MDPI and/or the editor(s). MDPI and/or the editor(s) disclaim responsibility for any injury to people or property resulting from any ideas, methods, instructions or products referred to in the content.